Chemotherapy-derived inflammatory responses accelerate the formation of immunosuppressive myeloid cells in the tissue microenvironment of human pancreatic cancer

Shintaro Takeuchi[1,2], Muhammad Baghdadi[2] , Takahiro Tsuchikawa[1], Haruka Wada[2], Toru Nakamura[1], Hirotake Abe[1,2], Sayaka Nakanishi[2], Yuu Usui[2], Kohtaro Higuchi[2], Mizuna Takahashi[1], Kazuho Inoko[1], Syoki Sato[1], Hironobu Takano[1], Toshiaki Shichinohe[1], Ken-ichiro Seino[2*] and Satoshi Hirano[1*]

[1] Department of Gastroenterological Surgery II, Hokkaido University Graduate School of Medicine, Kita-15, Nishi-7, Sapporo 060-8638, Japan

[2] Division of Immunobiology, Institute for Genetic Medicine, Hokkaido University, Kita-15 Nishi-7, Sapporo 060-0815, Japan

[*]Corresponding authors:

Ken-ichiro Seino, MD, PhD

Division of Immunobiology, Institute for Genetic Medicine, Hokkaido University

Kita-15, Nishi-7, Sapporo 060-0815, Japan

Tel: 81-11-706-5532

20 Fax: 81-11-706-7545

21 E-mail: seino@igm.hokudai.ac.jp

22

23 Satoshi Hirano, MD, PhD

24 Department of Gastroenterological Surgery II, Graduate School of Medicine,

25 Hokkaido University

26 Kita-15, Nishi-7, Sapporo 060-8638, Japan

27 Tel: 81-11-706-7714

28 Fax: 81-11-706-7158

29 E-mail: satto@med.hokudai.ac.jp

Abstract

Pancreatic ductal adenocarcinoma (PDAC) is the most common type of pancreatic malignancies. PDAC builds a tumor microenvironment that plays critical roles in tumor progression and metastasis. However, the relationship between chemotherapy and modulation of PDAC-induced tumor microenvironment remains poorly understood. In this study, we report a role of chemotherapy-derived inflammatory response in the enrichment of PDAC microenvironment with immunosuppressive myeloid cells. GM-CSF is a major cytokine associated with oncogenic KRAS in PDAC cells. GM-CSF production was significantly enhanced in various PDAC cell lines or PDAC tumor tissues from patients after treatment with chemotherapy, which induced the differentiation of monocytes into myeloid derived suppressor cells (MDSCs). Furthermore, blockade of GM-CSF with monoclonal antibodies helped to restore T cell proliferation when co-cultured with monocytes stimulated with tumor supernatants. GM-CSF expression was also observed in primary tumors and correlated with poor prognosis in PDAC patients. Together, these results describe a role of GM-CSF in the modification of chemotherapy-treated PDAC microenvironment, and suggest that the targeting of GM-CSF may benefit PDAC patients' refractory to current anticancer regimens by defeating MDSCs-mediated immune escape.

Introduction

Pancreatic ductal adenocarcinoma (PDAC) is an aggressive cancer characterized by high mortality and poor prognosis, where in advanced cases the average of life expectancy is less than 1 year (1, 2). A recent study of cancer incidence and mortality has projected PDAC to become the second leading cause of cancer-related death by 2030 in the United States (3). In spite of recent progress in treatment strategies, the current protocols of chemotherapy regimens remain insufficient to cure the patients (4, 5). Recently, we and other groups have reported a new concept of “Adjuvant surgery” in which PDAC patients are treated with pre-operative chemotherapy, followed by surgical resection which contributes to long term survival for locally advanced cases (6, 7). Unfortunately, this procedure can be applied in only a small population of selected patients that were characterized with high outcome of pre-operative chemotherapy (6, 7). Thus, new therapeutic strategies for improving chemotherapeutic response are critically needed to improve the clinical outcomes in advanced PDAC, which in turn depend on the deep understanding of changes induced in tumor microenvironment under chemotherapeutic conditions. In this context, it has recently become clear that anti-cancer chemotherapeutic agents can modify the tumor microenvironment, and the therapeutic effects mediated by these agents are considerably dependent on the host immunological reaction (8, 9). Additionally, the complex interaction between tumor cells and other cellular

components of tumor microenvironment such as cancer associated fibroblasts (CAF) and myeloid cells has great impact on invasion, metastasis and acquiring of chemo-resistant phenotypes (10, 11). PDAC microenvironment constitutes of molecular and cellular components with inflammatory features, such as pancreatic stellate cells (PaSC) and immune cells which affect PDAC progress (12, 13). Accumulating evidence has unveiled the role of KRAS oncogene in the formation of desmoplastic and inflammatory microenvironment via the secretion of multiple cytokines and chemokines (14). Thus, the understanding of the interaction between tumor microenvironment and immune cell and cytotoxic therapies is essential for the improvement of PDAC treatment.

Myeloid-derived suppressor cells (MDSCs) are heterogeneous populations of immune cells derived from progenitor cells in bone marrow, which accumulate in tumor microenvironment via various pathological mechanisms, and contribute to tumor progression by damping T-cell immunity and promoting angiogenesis (15, 16). Cytokines such as colony stimulating factors (e.g. GM-CSF and G-CSF) are key molecules involved in the generation of MDSCs (17, 18). Oncogenic *KRAS* is the most frequently mutated gene in PDAC and has been shown to be involved in PDAC development and growth (19, 20). Importantly, Oncogenic *KRAS* is associated with overexpression of GM-CSF which induces MDSCs formation in PDAC

88 microenvironments, which in turn prompt the development and progression of PDAC
89 in genetically engineered mouse models (21, 22). Moreover, targeted depletion of
90 MDSCs was effective to increase the intra-tumoral accumulation of activated T-cells
91 and thus improved the therapeutic efficacies of immunotherapy in murine models of
92 PDAC and other cancers (23). However little is known about the role of MDSCs in
93 human PDAC, especially in clinical therapeutic settings, for example, chemotherapy
94 treated conditions.
95 In the present study, we show phenotypic and functional changes of monocytes
96 under chemotherapy-treated human PDAC conditions. Human monocytes
97 differentiated into HLA-DR$^{low/negative}$ MDSC phenotype when cultured in conditioned
98 medium of human PDAC cells. Moreover, HLA-DR$^{low/negative}$ cells formation was
99 enhanced when human monocytes were cultured in conditioned medium of
100 chemotherapy-treated human PDAC cells. Gene and protein expression of GM-CSF
101 or other inflammatory factors in human PDAC cell lines were upregulated after
102 treatment with anticancer cytotoxic agents such as gemcitabine and Fluorouracil.
103 Blockade of GM-CSF in the supernatants of PDAC cell culture with specific
104 monoclonal antibodies resulted in recovery of T cell proliferation when co-cultured
105 with monocytes stimulated with PDAC conditioned medium. Consistent with these
106 results, we found that PDAC tumor tissues in chemotherapy-treated cancer patients

recruited more cells which express MDSC markers compared to non-treated group.

In conclusion, targeting of PDAC with chemotherapy may activate inflammatory signals that induce the production of multiple sets of cytokines and chemokines in tumor cells. Among these, GM-CSF has emerged as a critical factor that link inflammatory signals with the creation of immunosuppressive microenvironment via the acceleration of monocytes differentiation into MDSCs. Together, our results give a new insight into how chemotherapy may results in counterproductive effects, and highlight the candidate molecules to be targeted in future improvement of PDAC treatment.

Materials and Methods

Ethics

Human PDAC samples were obtained from surgical specimens after obtaining informed consent from all patients. Blood samples were obtained from healthy volunteers and PBMCs were separated using cell separating tube (BD Bioscience). Both procedures were ethically approved by the committees in the Institutional review Board of Hokkaido University Hospital (No. 013-0389, 013-0390).

Human PDAC tissue samples

For tissue microarray (TMA), PDAC tissue samples were obtained from 99 resected PDAC in our institute between 1994 and 2005. TMA was constructed as described in our previous report (24). Patients without information about survival or broken and poor samples were omitted from analysis. Total 68 patients were subjected to analysis. The characteristics of patients for TMA study are summarized in supplementary table 1. Evaluation procedure was performed as previously reported with a little modification. The intensity of GM-CSF staining was classified according to a three-level scale: 0 = weak or equivalent staining compared with normal pancreas, 1+ = strong and partial staining to cytoplasm of cancer cell, 2+ = strong and diffuse staining to cytoplasm. Scoring was evaluated by two independent investigators.

The 15 patients that were evaluated in the comparison study (figure 5) are overlap cohorts described in our previous report resected in our institute between 2006 and 2010 (25). The characteristics of these patients are summarized in supplementary table 2-3. Immunohistochemistry testing and evaluation of myeloid cells were performed according to previous reports (25). Briefly, five areas of most abundant myeloid cells distribution were selected in high-power field (×400). Average counted numbers of areas were compared. All specimens were evaluated by two independent investigators.

Cell lines

Human PDAC cell lines (Capan-1, Capan-2, PANC-1, MIAPaCa-2, and BxPC-3), human cervical cancer cell line (HeLa) and human leukemia cell line (Jurkat) were purchased from ATCC. PK-45-P and PK-1 were purchased from RIKEN. PCI-43 and PCI-43-P5 were previously established from surgically resected primary carcinoma tissues in our institute (26). All cell lines were cultured in an appropriate medium as indicated by manufactures or references. For conditioned medium used in monocyte culture, Capan-1 and PANC-1 cells were cultured in RPMI 1640 (WAKO) supplemented with 10% fetal bovine serum (Cell Culture Bioscience), 1% penicillin/streptomycin, 10mM HEPES, 1% L-glutamine, 1mM sodium pyruvate, 1%

non-essential amino acids (All from Life technologies), and 50μM 2-mercaptoethanol (WAKO) in accordance with optimizing conditions for monocytes.

In vitro human monocyte culture

To examine the effects of PDAC-derived factors on monocytes differentiation, we established the following *in vitro* models. For normal condition, the supernatants of PDAC cell culture were harvested when cells became 80% confluent, and passed through 0.2μm filter (Sartourius Stedim Biotech). To mimic clinical pharmacological settings in PDAC patients, gemcitabine (GEM, 1-30μM) or fluorouracil (5-FU, 10μg/ml) were applied at concentrations similar to that used in clinic (1-30μM). PDAC cells were pulsed with GEM or 5-FU for 60 minutes followed by wash for 5 times with sterilized PBS and change to fresh media. After 72 hours, supernatants were collected and passed through 0.2μm filter as described above. Human peripheral monocytes were purified from PBMC of healthy donors using CD14 positive selection by magnetic cell sorting systems according to manufacture' s protocols (Miltenyi Biotech) and cultured in the presence of supernatants prepared from normal PDAC or chemotherapy-treated PDAC cells for 6 days. On day 6, gene expression and protein analysis were evaluated by quantitative RT-PCR or flow cytometry, respectively. In some experiments, cytokines in the supernatants of PDAC cell culture were

neutralized using anti-human GM-CSF (Clone BVD2-23B6; Biolegend, 10μg/ml), anti-human IL-6 (Clone 6708; R&D systems, 2μg/ml), or anti-human IL-8 (Clone 6217; R&D systems, 2μg/ml).

Flow cytometry

Single cell suspensions were used for flow cytometry analysis after treatment with Human FcR blocker (Miltenyi Biotech) or anti-mouse CD16/32 (BD Biosciences) and staining with appropriate fluorescent antibodies according to manufacturer's instruction. Fluorescent antibodies used for the staining of human cell surface markers were purchased from BD Biosciences (anti-HLA-DR and anti-CD15), BECKMAN COULTER (anti-CD11b and anti-CD33), Miltenyi Biotec (anti-CD14) or Biolegend (anti-CCR2 and anti-CX3CR1). Fluorescent antibodies used for the staining of mouse cell surface markers were purchased from Biolegend (anti-CD11b and anti-Gr1). Samples were run on FACS canto II (BD Biosciences) and analysed using FlowJo software V7.6.5

Quantitative RT-PCR

RNA was extracted from cells using RNeasy Plus Mini Kit (QIAGEN) according to the manufacturer's protocol, and used for cDNA synthesis (Prime Script RT Master Mix,

192 TAKARA BIO). cDNA products were used to amplify target genes using Power SYBR
193 Green (Life Technologies) and specific primer (Supplementary Table 3). PCR
194 reactions and data analysis were performed in a StepOne Real-time PCR system
195 (Applied Biosystems), using the comparative C_T method and the housekeeping gene
196 *GAPDH*. Primers used in this study are as follows:
197 *GAPDH* (Forward: 5'-AACAGCGACACCCACTCCTC-3' Reverse:
198 5'-ATACCAGGAAATGAGCTTGACAA-3'), *M-CSF* (Forward:
199 5'-GCCTGCGTCCGAACTTCTA-3' Reverse: 5'-ACTGCTAGGGATGGCTTTGG-3'),
200 *GM-CSF* (Forward: 5'-ATGATGGCCAGCCACTACAA-3' Reverse:
201 5'-CTGGCTCCCAGCAGTCAAAG-3'), *IL-6* (Forward:
202 5'-GGCACTGGCAGAAAACAACC-3' Reverse: 5'-GCAAGTCTCCTCATTGAATCC-3),
203 *IL-8* (Forward: 5'-CTGCGCCAACACAGAAAATTA-3' Reverse:
204 5'-ATTGCATCTGGCAACCTAC-3'), *IL-1B* (Forward:
205 5'-ATCACTGAACTGCACGTCC-3' Reverse: 5'-GCCCAAGGCCACAGGTATTT-3'),
206 *PTCS2* (Forward: 5'-GTTCCACCCGCAGTACAGAA-3' Reverse:
207 5'-AGGGCTTCAGCATAAAGCGT-3'), *TNF* (Forward:
208 5'-CACAGTGAAGTGCTGGCAAC-3' Reverse: 5'-AGGAAGGCCTAAGGTCCACT-3'),
209 *VEGF-A* (Forward: 5'-CTACCTCCACCATGCCAAGT-3', Reverse:
210 5'-GCAGTAGCTGCGCTGATAGA-3'), *CXCL-12* (Forward:

211 5'-CTACAGATGCCCATGCCGAT-3' Reverse: 5'-CAGCCGGGCTACAATCTGAA-3'),

212 *SCF* (Forward: 5'-AGCCAGCTCCCTTAGGAATGA-3' Reverse:

213 5'-TGCCCTTGTAAGACTTGGCTG-3'), *TGF-B1* (Forward:

214 5'-GGGACTATCCACCTGCAAGA-3' Reverse: 5'-GAACCCGTTGATGTCCACTT-3'),

215 *CCL-2* (Forward: 5'-CAGCAAGTGTCCCAAAGAAGCTG-3' Reverse:

216 5'-TGGAATCCTGAACCCACTTCTGC-3'), *NOS2* (Forward:

217 5'-TCCAAGGTATCCTGGAGCGA-3' Reverse: 5'-AATGTGGGGCTGTTGGTGAA-3'),

218 *ARG1* (Forward: 5'-ATGTTGACGGACTGGACCCATCT-3' Reverse:

219 5'-TGCAACTGCTGTGTTCACTGTTC-3'), *IL-10 (Forward:*

220 5'-GAGATGCCTTCAGCAGAGTGA-3' Reverse:

221 5'-ACATGCGCCTTGATGTCTGG-3'). Primers specificity was confirmed by peak melt

222 curve before using. All experiments were performed in duplicate for each sample.

223

224 ***Cytokine measurement***

225 Cytokines were measured using commercial ELISA kits according to the

226 manufacturer's instructions. The kits for GM-CSF and IL-8 were purchased from

227 Biolegend. The kit for IL-6 was purchased from R&D systems. All measurements were

228 performed using supernatants from three independent cell cultures.

229

Western blotting

Total cell lysates were prepared using RIPA buffer supplemented with protease inhibitors aprotinin and PMSF. Protein samples were resolved using 10% SDS-PAGE and were then transferred to PVDF membrane (GE Healthcare). Membranes were probed with primary antibodies against target molecules followed by reaction with secondary antibodies conjugated to horseradish peroxidase (HRP) for appropriate incubation time. Antibodies against ERK, p-ERK, AKT and p-AKT were purchased from Cell Signaling; antibodies against β-Actin were purchased from Millipore; secondary antibodies were purchased from Jackson ImmunoResearch. Immunoreactivity was detected by an enhanced chemiluminescence detection system (GE Healthcare). Equal loading of proteins was confirmed with β-Actin.

NF-κB luciferase reporter assay

Promoter activities of *NF-κB* in cultured cells were monitored using Ready-To-Glow^{TM} secreted luciferase reporter system (Clontech). Briefly, Capan-1 cells were transfected with secreting luciferase reporter plasmid encoding NF-κB using Lipofectamine 2000 (Invitrogen), and stable clones were selected by G418. Stable clones were stimulated with GEM or 5-FU and luciferase activities in the supernatants were detected at the indicated time points. Luciferase activities were

compensated by cell number.

T-cell proliferation assay

Autologous reactions of monocytes and $CD4^+$ or $CD8^+$ T cells were estimated by ^{3}H-thymidine incorporation assay. Briefly, human $CD4^+$ or $CD8^+$ T cells were isolated from PBMC of healthy donors using $CD4^+$ T cell isolation kit and $CD8^+$ T cell isolation kit (Miltenyi Biotec). $CD4^+$ or $CD8^+$ T cells were cultured in the presence of 3μg/ml of anti-CD3 antibody (OKT3; eBioscience) and 1μg/ml of anti-CD28 antibody (CD28.2; Biolegend). Stimulated $CD4^+$ or $CD8^+$ T cells were then co-cultured with monocytes differentiated in the presence of tumor supernatants at the indicated conditions at different T cell / monocyte ratios. ^{3}H-thymidine incorporations were counted after 72 hours culture.

Immunohistochemical staining of formalin fixed paraffin embedded tissues (FFPE)

Paraffin-embedded specimens were cut into thin slices and mounted on slide glass. Sections were deparaffinized in xylene, and rehydrated in ethanol. Antigen retrieval was performed by boiling for 20 minutes in citrate buffer (pH 6.0) or Tris-EDTA buffer (pH 9.0). Endogenous peroxidase activity was blocked with 3% hydrogen peroxide in

methanol. Nonspecific reactions were blocked with original blocking cocktails; the equal quantity of 10% normal goat serum (Nichirei), Protein-Block Serum-Free Ready-To-Use (DAKO), and antibody diluent with background reducing components (DAKO). Immunohistochemical reactions were carried out using the enzyme polymer methods with Histofine series (Nichirei). Primary antibodies were mounted into slides for 60 minutes at room temperature or overnight at 4℃ followed by 20 minutes incubation with secondary antibodies at room temperature. Antibodies used for FFPE were purchased from LSBio (GM-CSF: LS-C104671 clone), Abcam (CD14: ab49755 clone, HLA-DR: EPR3692 clone) and Biolegend (CD66b: G10F5), and used according to the manufacturer's instructions. The list of primary antibodies with their reactive conditions is listed in supplementary table 4. Immunohistochemical reactions were visualized with DAB or Fast Red II (Nichirei) followed by counterstaining with hematoxylin and mounted on coverslips.

Statistical analysis

Parametric statistics were applied for *in vitro* data and Student's *t*-test was used for comparison between groups. For mouse or human data, non-parametric statistics were applied in which Man-Whitney *U* test, Fisher's exact test, or χ^2 test were used as appropriate. Overall survival was calculated from the date of operation to the date of last follow-up or date of patient death. The Kaplan-Meier method was used to

287 estimate overall survival, and survival differences were estimated by the log-rank test.

288 Except where indicated, the values were presented as mean ± SEM. *P* was

289 considered statistically significant when < 0.05. All data were analyzed using StatFlex

290 software v6.0.

Results

Human monocytes differentiate into MDSCs when cultured in the supernatants of PDAC cell culture

PDAC cells secrete multiple inflammatory cytokines and growth factors. To assess how PDAC cells-derived soluble factors influence human myeloid cells differentiation, we generated *in vitro* culture models using conditioned medium (CM) from 2 PDAC cell lines: Capan-1 and PANC-1 (Figure 1A). We found that human monocytes formed different morphologies in response to PDAC tumor supernatants. Monocytes differentiated into spindle adherent cells when cultured in normal medium, while monocytes that were differentiated in the presence of Capan-1 or PANC-1 supernatants formed floating immature cells (Figure 1B). Previous reports suggested that PDAC induces the accumulation of MDSCs in tumor regions in genetically engineered mouse models (21, 22). Monocyte-derived MDSCs (Mo-MDSCs) from cancer patients express the monocyte-macrophage marker CD14 and the common myeloid marker CD33, but lack or show lower expression of mature myeloid markers HLA-DR (27). We found that human monocytes expressed CD14 and CD33, while HLA-DR expression was relatively lower in monocytes cultured in the presence of PDAC supernatants compared to normal medium (Figure 1C and 1D). Mo-MDSCs suppress T cell immunity via nitric oxide synthase 2 (NOS2) or Arginase 1 (ARG1) (28,

29). Thus, we next evaluated the expression levels of these two enzymes in monocytes induced by PDAC CM. PDAC CM-treated monocytes showed high expression of both NOS2 and ARG1 (Figure 1E). Additionally, we examined the expression of other myeloid lineage markers, and found that PDAC CM-treated monocytes express the common myeloid marker CD11b, chemokine receptor 2 (CCR2), but lack the expression of granulocyte or tissue resident macrophage marker CD15 or CX3C chemokine receptor 1 (CX3CR1) (30) (Figure 1F). Together, these data demonstrated that human peripheral monocytes differentiated into mo-MDSCs when stimulated with PDAC CM.

The supernatants of chemotherapy-treated PDAC cells enhance the differentiation of human monocytes into MDSCs

Next, we examined if the differentiation patterns of monocytes are altered in chemotherapy-treated PDAC microenvironment. To do so, we established *in vitro* culture model using Capan-1 cell line treated with gemcitabine (GEM) or Fluorouracil (5-FU) (Figure 2A). Interestingly, after 6 days of culture, monocytes showed morphological changes when cultured in the supernatants of chemotherapy-treated PDAC cells, represented by increased diameters (Figure 2B and Supplementary Fig. S1) and formation of cytoplasmic vacuoles that were not observed in monocytes

cultured in normal medium or normal PDAC supernatant (Figure 2C). These monocytes showed high forward and side scatter voltage signals in flowcytometry analysis, which was consistent with gross examination (Figure 2D). Additionally, the HLA-DR$^{low/negative}$ fraction was increased in monocytes differentiated in the supernatants of chemotherapy-treated PDAC cells (Figure 2D, E and Supplementary Fig. S1). These changes are consistent with the phenotype of HLA-DR$^{low/negative}$ immature monocytes that have been previously reported (27). To evaluate the immunosuppressive features of monocytes differentiated in GEM-treated PDAC CM, we analysed expression levels of *ARG1*, *IL-10*, *TGF-β1* and *NOS2.* Although no significant changes were observed in the expression of *ARG1*, *IL-10* or *TGF-β1* (data not shown), *NOS2* expression was significantly increased in monocytes differentiated in GEM-treated PDAC CM (Figure 2F). MDSCs are usually characterized by lack or low expression of HLA-DR, and high expression of *NOS2* (28, 31). Accordingly, these data suggest that the supernatants of chemotherapy-treated PDAC cells accelerate the differentiation of monocytes into MDSCs with enhanced molecular patterns.

Treatment with chemotherapy amplifies the expression of GM-CSF and other inflammatory cytokines in PDAC cells via the activation of MAPK signalling pathway and NF-κB transcription

MDSCs are immunosuppressive myeloid cells that contribute to tumor progression and immune evasion. Accumulating evidence has unveiled that GM-CSF and other tumor-derived molecules are necessary for the induction of preferential expansion of MDSCs in tumor microenvironment (33, 34). To identify factors in the supernatants of chemotherapy-treated PDAC cells responsible for monocytes differentiation into MDSCs, we investigated expression profiles of various cytokine and chemokine in Capan-1 or PANC-1 cell lines. Following stimulation with GEM or 5-FU, several cytokines and chemokines were upregulated in both cell lines (Figure 3A, B and Supplementary Fig. S2). In particular, the expression of GM-CSF, IL-6 and IL-8 was increased in the supernatants of chemotherapy-treated Capan-1 cells (Figure 3C, Supplementary Fig. S3). In the next experiment, we focused on GM-CSF since both cell lines showed a significant enhancement in GM-CSF production after treatment with GEM or 5-FU. In addition, GM-CSF is well known for its role as an essential factor of MDSC proliferation and differentiation in PDAC (22). In oncogenic KRAS-mediated PDAC murine model, GM-CSF is regulated by MAPK or PI3K signalling pathway, two major downstream pathways of KRAS oncogene (21). Thus we next compared the activation status of these two pathways through the evaluation of ERK phosphorylation as an indicator for MAPK pathway, or AKT for PI3K pathway in normal or chemotherapy-treated conditions. We found that GEM treatment enhances

367 the phosphorylation of ERK (Figure 3D) but not AKT (data not shown) in a
368 time-dependent manner. NF-κB is a major transcription factor which induces the
369 expression of inflammatory cytokines including GM-CSF (35, 36). Thus, we next
370 examined if GEM treatment may induce promoter activities of NF-κB in PDAC cells. In
371 a luciferase assay, we found that NF-κB-luciferase activities were enhanced after
372 chemotherapy treatment (Figure 3E). These data indicate that chemotherapy
373 enhances the production of multiple inflammatory cytokines including GM-CSF by
374 amplifying the activation status of MAPK signalling pathway and NF-κB promoter
375 activities in PDAC cells.
376
377 ***Neutralization of GM-CSF in the supernatants of chemotherapy-treated PDAC***
378 ***cells blocks monocytes differentiation into MDSCs and help recovery of T cell***
379 ***proliferation***
380 The supernatants of chemotherapy-treated PDAC cells were enriched with GM-CSF,
381 and induced morphological and phenotypic changes in monocytes. To further
382 examine the contribution of GM-CSF in these changes, we utilized a specific
383 monoclonal antibody to neutralize GM-CSF in chemotherapy-treated Capan-1 CM.
384 Interestingly, we found that the neutralization of GM-CSF has resulted in decreased
385 forward and side scatter voltage signals as well as HLA-DR$^{low/negative}$ fractions (Figure

386 4A), and abolished the formation of cytoplasmic vacuoles that were observed in the
387 case of GEM-treated Capan-1 CM (Figure 4B). These data indicate that GM-CSF is
388 one of the major factors of monocyte differentiation in the supernatants of
389 chemotherapy-treated PDAC cells.

390 MDSCs are heterogeneous populations of cells that are defined by their ability to
391 potently suppress T cell response by NOS2-dependent mechanism (31). As described
392 above, the supernatants of chemotherapy-treated PDAC cells were enriched with
393 GM-CSF, and induced high expression of NOS2 in MDSCs differentiated from
394 monocytes. To confirm the immunosuppressive potential of MDSCs generated from
395 monocytes in the presence of PDAC supernatants, we co-cultured these MDSCs with
396 $CD4^+$ or $CD8^+$ T cells and examined T cell aggregation and proliferation after
397 stimulation. Interestingly, MDSCs generated from monocytes by normal Capan-1 CM
398 suppressed aggregation and proliferation of stimulated $CD4^+$ or $CD8^+$ T cells, which
399 was further suppressed by MDSCs generated by GEM-treated Capan-1 CM (Figure
400 4C, D and Supplementary Fig. S4). Importantly, the neutralization of GM-CSF in
401 GEM-treated Capan-1 CM was effective to abolish these immunosuppressive
402 functions and contribute to the recovery of T cell function as observed by enhanced
403 aggregation and proliferation (Figure 4C, D and Supplementary Fig. S4). Together,
404 these data highlight the role of GM-CSF in the enhancement of MDSCs formation in

405 chemotherapy-treated PDAC microenvironment, and suggest that the neutralization
406 of GM-CSF may contribute to block the formation of MDSCs and thus the recovery T
407 cell response.
408
409 ***GM-CSF is expressed in various human PDAC cell lines and tumor tissues and***
410 ***serves as a poor prognostic indicator for PDAC patients***
411 To investigate whether GM-CSF expression is a common feature of PDAC cells, we
412 examined the expression of GM-CSF in human samples. Quantitative PCR analysis
413 showed high expression of GM-CSF in all PDAC cell lines with some variations
414 (Figure 5A). Next, immunohistochemistry staining was used to examine protein levels
415 of GM-CSF in PDAC tissues of 68 resected primary tumors by tissue microarray.
416 PDAC tissues also showed variety in GM-CSF expression (Figure 5B). The intensity
417 of GM-CSF staining was classified as high or low as described in material and
418 methods (Figure 5B and C), and scores were used to generate Kaplan-Meier survival
419 curve. We found that survival rates were significantly lower in patients with high
420 expression of GM-CSF (Figure 5D). These data suggest that GM-CSF, a MDSC
421 inducing cytokine, is generally expressed in human PDAC, and correlate with poor
422 prognosis.
423 Finally, to examine the impact of tumor microenvironment on MDSCs differentiation

424 in human PDAC tissues under chemotherapeutic conditions, we assessed MDSC
425 marker expression in tumor-infiltrating myeloid cells in PDAC patients treated with
426 pre-operative chemotherapy including GEM in our institute (Supplementary table 3).
427 We found that tumor-infiltrating $CD14^+$ cells in PDAC patients treated with
428 pre-operative chemotherapy show no or weak expression of HLA-DR compared to
429 patients without pre-operative chemotherapy treatment (Figure 5E and F). These data
430 indicate that $CD14^+HLA\text{-}DR^-$ cells constitute a dominant fraction in PDAC tissues
431 following chemotherapy. Furthermore, we investigated the expression of CD66b, a
432 marker of granulocytic MDSC (G-MDSC) (38), and found that the frequencies of
433 tumor-infiltrating $CD66b^+$ cells were significantly higher in PDAC patients after
434 chemotherapy treatment (Figure 5G and H). On the other hand, no significant
435 difference was observed in the frequencies of $CD68^+$ macrophages between the two
436 groups (Supplementary Fig. S5). Taken together, these results suggest that
437 chemotherapy treatment accelerates the formation of both Mo-MDSCs and G-MDSCs
438 in human PDAC tissues, in consistent with previous experiments.

Discussion

Most of PDAC cancer cases are diagnosed at late stages, which make surgical resection of the tumor or the organ difficult if not impossible (39). Chemotherapy has been suggested as a possible strategy for the treatment of PDAC patients; however clinical response mediated by anticancer cytotoxic agents against PDAC is so limited, and it is unlikely that chemotherapy alone will provide durable clinical benefit for the majority of PDAC patients. Thus, new combination protocols are suggested to gain cumulative or synergistic benefit in large population of patients. One good example is the treatment with radical surgery, which was accompanied by favourable clinical outcomes in some clinical cases (6, 7). Moreover, recent progress has been achieved in the protocols of “neoadjuvant chemotherapy” against PDAC (40, 41). These new protocols enable the analysis of molecular and pathological patterns of chemotherapy-treated PDAC. For example, recent pre-operative chemotherapy protocols helped to identify the molecular patterns of T cells, showing increased accumulation in tumor tissues in PDAC or oesophageal cancer patients (25,42,43). Additionally, in this study we have reported for the first time the distribution of MDSC markers in PDAC patients after chemotherapy treatment, in which MDSCs were the dominant cells in cancer regions. However, the real therapeutic effects of chemotherapy in PDAC treatment still poorly understood, since a large proportion of

458 PDAC patients develop chemoresistance and thus cannot receive surgical therapy.
459 Therefore, further studies are critically needed to identify the molecular mechanism of
460 chemoresistance in PDAC.

461 It is now well established that the antitumor activities of chemotherapy considerably
462 rely on the complex interaction between tumor and immune system of the host (9, 44).
463 Moreover, accumulating evidence has unveiled the importance of the interaction
464 between tumor cells and myeloid cells in inducing chemoresistance and metastasis
465 (11, 45). This is also applicable in the case of PDAC, and the deep understanding of
466 this complex interaction in tumor microenvironment is a key concept for the
467 improvement of chemotherapeutic response against PDAC. To understand how
468 PDAC cells influence tumor microenvironment in chemotherapy-treated condition, we
469 first analysed monocyte differentiation patterns using *in vitro* culture models. When
470 stimulated with the supernatants of chemotherapy-treated PDAC cells, human
471 monocytes differentiated into immunosuppressive cells that resemble MDSCs,
472 showing similar morphology and shared the same molecular markers. Interestingly,
473 the supernatants of chemotherapy-treated PDAC cells were found to be enriched with
474 GM-CSF and other inflammatory factors which induce the differentiation of monocytes
475 into MDSCs. Consistent with this, immunostaining of tumor tissues of PDAC patients
476 treated with chemotherapy has shown enhancement in MDSC markers compared to

normal tissues. Thus, chemotherapy itself may result in counterproductive effects in which the formation of immunosuppressive and tumorigenic myeloid cells is enhanced at the microenvironment of PDAC.

MDSCs are a heterogeneous population of immature myeloid cells that negatively regulate the anti-tumor immune responses (15). MDSCs also support tumor immune evasion by suppressing T cell immunity, and promote angiogenesis and tumor progression (21, 22, 46). Accumulation of MDSCs has been correlated with tumor progression in patients (39). Additionally, a recent report has suggested that MDSCs contribute to senescence evasion and chemoresistance in tumor (11). In PDAC, MDSCs were found to be induced by MAPK or PI3K pathway-dependent GM-CSF, and significantly correlated with tumor development and prognosis (21, 22). Importantly, we have found that GM-CSF production was dramatically enhanced in several PDAC cell lines as well as tumor tissues in PDAC patients after treatment with chemotherapy, which was accompanied by increased frequencies of MDSCs. One possible mechanism is the activation of MAPK and NF-κB signalling pathway as a consequent of chemotherapy-induced DNA-damage response (DDR) (47). However, detailed mechanism should be elucidated in future studies.

GM-CSF may play two different roles at the tumor microenvironment of PDAC. First, GM-CSF may help to induce or activate anticancer immune responses through the

496 priming of immunostimulatory dendritic cells (DC). Based on this concept, GVAX®, a
497 GM-CSF gene-transferred tumor cell vaccine, has been developed for the treatment
498 of advanced PDAC patients, but the clinical outcome was lower than what was
499 expected (48). Alternatively, GM-CSF may induce the formation of MDSC. One
500 possible mechanism of these conflict roles of GM-CSF is the enrichment of PDAC
501 microenvironment with DAMPs (Danger-associated molecular patterns) after
502 chemotherapy treatment. DAMPs are released from tumor cells killed by anticancer
503 cytotoxic agents, and signalling mediated by these DAMPs may be involved in the
504 alteration of cellular differentiation pattern (49, 50), which should be clarified in future
505 studies.

506 Our data indicate that MDSCs were increased after treatment of PDAC with
507 chemotherapy, which was related to enhancement in GM-CSF production. The
508 neutralization of GM-CSF with antibodies was effective to reduce MDSC frequencies,
509 and help the recovery of T cell function (Figure 6). Depletion of MDSCs has been
510 recently suggested for PDAC treatment (23). In this context, the targeting of GM-CSF
511 may constitute an additional option to further improve current protocols of PDAC
512 treatment.

513 In conclusion, our data identify a role of chemotherapy-derived inflammatory
514 response, in particular GM-CSF, in the enrichment of PDAC microenvironment with

MDSCs. Here we suggest that the targeting of MDSCs by direct depletion and / or the neutralization of tumor-derived GM-CSF in combination with current therapeutic regimens constitute a promising strategy for the treatment of PDAC patients.

Disclosure statement

No potential conflicts of interest were disclosed.

Acknowledgments

The authors thank Hiraku Shida for technical assistance in making slides for immunochemical staining, and Tomohiro Shimizu and Katsuji Marukawa for kindly supporting in cytospin techniques. Finally, the authors would like to express heartful thanks to the later Dr. Masaki Miyamoto for the guidance and mentorship of this research.

References

1. Siegel, R., Ma, J., Zou, Z., and Jemal, A. 2014. Cancer statistics, 2014. *CA: A Cancer Journal for Clinicians* 64: 9-29.
2. Shaib, Y.H., Davila, J.A., and El-Serag, H.B. 2006. The epidemiology of pancreatic cancer in the United States: changes below the surface. *Alimentary Pharmacology & Therapeutics* 24: 87-94.
3. Rahib, L., Smith, B.D., Aizenberg, R., Rosenzweig, A.B., Fleshman, J.M., and Matrisian, L.M. 2014. Projecting Cancer Incidence and Deaths to 2030: The Unexpected Burden of Thyroid, Liver, and Pancreas Cancers in the United States. *Cancer Research* 74: 2913-2921.
4. Conroy, T., Desseigne, F., Ychou, M., Bouché, O., Guimbaud, R., Bécouarn, Y., Adenis, A., Raoul, J.-L., Gourgou-Bourgade, S., de la Fouchardière, C., et al. 2011. FOLFIRINOX versus Gemcitabine for Metastatic Pancreatic Cancer. *New England Journal of Medicine* 364: 1817-1825.
5. Paulson, A.S., Tran Cao, H.S., Tempero, M.A., and Lowy, A.M. 2013. Therapeutic Advances in Pancreatic Cancer. *Gastroenterology* 144: 1316-1326.
6. Kato, K., Kondo, S., Hirano, S., Tanaka, E., Shichinohe, T., Tsuchikawa, T., and Matsumoto, J. 2011. Adjuvant surgical therapy for patients with

545 initially-unresectable pancreatic cancer with long-term favorable responses to
546 chemotherapy. *Journal of Hepato-Biliary-Pancreatic Sciences* 18: 712-716.
547 7. Satoi, S., Yamaue, H., Kato, K., Takahashi, S., Hirono, S., Takeda, S., Eguchi, H.,
548 Sho, M., Wada, K., Shinchi, H., et al. 2013. Role of adjuvant surgery for patients
549 with initially unresectable pancreatic cancer with a long-term favorable response to
550 non-surgical anti-cancer treatments: results of a project study for pancreatic
551 surgery by the Japanese Society of Hepato-Biliary-Pancreatic Surgery. *Journal of*
552 *Hepato-Biliary-Pancreatic Sciences* 20: 590-600.
553 8. Galluzzi, L., Senovilla, L., Zitvogel, L., and Kroemer, G. 2012. The secret ally:
554 immunostimulation by anticancer drugs. *Nat Rev Drug Discov* 11: 215-233.
555 9. Andre, F., Dieci, M.V., Dubsky, P., Sotiriou, C., Curigliano, G., Denkert, C., and Loi,
556 S. 2013. Molecular Pathways: Involvement of Immune Pathways in the
557 Therapeutic Response and Outcome in Breast Cancer. *Clinical Cancer Research*
558 19: 28-33.
559 10. Quail, D.F., and Joyce, J.A. 2013. Microenvironmental regulation of tumor
560 progression and metastasis. *Nat Med* 19: 1423-1437.
561 11. Di Mitri, D., Toso, A., Chen, J.J., Sarti, M., Pinton, S., Jost, T.R., D/'Antuono, R.,
562 Montani, E., Garcia-Escudero, R., Guccini, I., et al. 2014. Tumour-infiltrating Gr-1+

563 myeloid cells antagonize senescence in cancer. *Nature* advance online
564 publication.
565 12. Apte, M.V., Wilson, J.S., Lugea, A., and Pandol, S.J. 2013. A Starring Role for
566 Stellate Cells in the Pancreatic Cancer Microenvironment. *Gastroenterology* 144:
567 1210-1219.
568 13. Zheng, L., Xue, J., Jaffee, E.M., and Habtezion, A. 2013. Role of Immune Cells
569 and Immune-Based Therapies in Pancreatitis and Pancreatic Ductal
570 Adenocarcinoma. *Gastroenterology* 144: 1230-1240.
571 14. di Magliano, M.P., and Logsdon, C.D. 2013. Roles for KRAS in Pancreatic Tumor
572 Development and Progression. *Gastroenterology* 144: 1220-1229.
573 15. Gabrilovich, D.I., and Nagaraj, S. 2009. Myeloid-derived suppressor cells as
574 regulators of the immune system. *Nat Rev Immunol* 9: 162-174.
575 16. Corzo, C.A., Condamine, T., Lu, L., Cotter, M.J., Youn, J.-I., Cheng, P., Cho, H.-I.,
576 Celis, E., Quiceno, D.G., Padhya, T., et al. 2010. HIF-1α regulates function and
577 differentiation of myeloid-derived suppressor cells in the tumor microenvironment.
578 *The Journal of Experimental Medicine* 207: 2439-2453.
579 17. Serafini, P., Carbley, R., Noonan, K.A., Tan, G., Bronte, V., and Borrello, I. 2004.
580 High-Dose Granulocyte-Macrophage Colony-Stimulating Factor-Producing

581 Vaccines Impair the Immune Response through the Recruitment of Myeloid
582 Suppressor Cells. *Cancer Research* 64: 6337-6343.
583 18. Lesokhin, A.M., Hohl, T.M., Kitano, S., Cortez, C., Hirschhorn-Cymerman, D.,
584 Avogadri, F., Rizzuto, G.A., Lazarus, J.J., Pamer, E.G., Houghton, A.N., et al.
585 2012. Monocytic CCR2+ Myeloid-Derived Suppressor Cells Promote Immune
586 Escape by Limiting Activated CD8 T-cell Infiltration into the Tumor
587 Microenvironment. *Cancer Research* 72: 876-886.
588 19. Iacobuzio-Donahue, C.A., Velculescu, V.E., Wolfgang, C.L., and Hruban, R.H.
589 2012. Genetic Basis of Pancreas Cancer Development and Progression: Insights
590 from Whole-Exome and Whole-Genome Sequencing. *Clinical Cancer Research*
591 18: 4257-4265.
592 20. Iacobuzio-Donahue, C.A. 2012. Genetic evolution of pancreatic cancer: lessons
593 learnt from the pancreatic cancer genome sequencing project. *Gut* 61: 1085-1094.
594 21. Pylayeva-Gupta, Y., Lee, Kyoung E., Hajdu, Cristina H., Miller, G., and Bar-Sagi,
595 D. 2012. Oncogenic Kras-Induced GM-CSF Production Promotes the
596 Development of Pancreatic Neoplasia. *Cancer Cell* 21: 836-847.
597 22. Bayne, Lauren J., Beatty, Gregory L., Jhala, N., Clark, Carolyn E., Rhim,
598 Andrew D., Stanger, Ben Z., and Vonderheide, Robert H. 2012. Tumor-Derived

599 Granulocyte-Macrophage Colony-Stimulating Factor Regulates Myeloid
600 Inflammation and T Cell Immunity in Pancreatic Cancer. *Cancer Cell* 21: 822-835.
601 23. Stromnes, I.M., Brockenbrough, J.S., Izeradjene, K., Carlson, M.A., Cuevas, C.,
602 Simmons, R.M., Greenberg, P.D., and Hingorani, S.R. 2014. Targeted depletion of
603 an MDSC subset unmasks pancreatic ductal adenocarcinoma to adaptive
604 immunity. *Gut*.
605 24. Tanaka, K., Tsuchikawa, T., Miyamoto, M., Maki, T., Ichinokawa, M., Kubota, K.C.,
606 Shichinohe, T., Hirano, S., Ferrone, S., Dosaka-Akita, H., et al. 2012.
607 Down-regulation of Human Leukocyte Antigen class I heavy chain in tumors is
608 associated with a poor prognosis in advanced esophageal cancer patients. Int J
609 Oncol 40:965-974.
610 25. Tsuchikawa, T., Hirano, S., Tanaka, E., Matsumoto, J., Kato, K., Nakamura, T.,
611 Ebihara, Y., and Shichinohe, T. 2013. Novel aspects of preoperative
612 chemo(radiation)therapy improving anti-tumor immunity in pancreatic cancer.
613 *Cancer Science*
614 26. Shichinohe, T., Senmaru, N., Furuuchi, K., Ogiso, Y., Ishikura, H., Yoshiki, T.,
615 Takahashi, T., Kato, H., and Kuzumaki, N. 1996. Suppression of Pancreatic
616 Cancer by the Dominant NegativerasMutant, N116Y. *Journal of Surgical Research*
617 66: 125-130.

27. Almand, B., Clark, J.I., Nikitina, E., van Beynen, J., English, N.R., Knight, S.C., Carbone, D.P., and Gabrilovich, D.I. 2001. Increased Production of Immature Myeloid Cells in Cancer Patients: A Mechanism of Immunosuppression in Cancer. *The Journal of Immunology* 166: 678-689.

28. Youn, J.-I., Nagaraj, S., Collazo, M., and Gabrilovich, D.I. 2008. Subsets of Myeloid-Derived Suppressor Cells in Tumor-Bearing Mice. *The Journal of Immunology* 181: 5791-5802.

29. Virtuoso, L.P., Harden, J.L., Sotomayor, P., Sigurdson, W.J., Yoshimura, F., Egilmez, N.K., Minev, B., and Kilinc, M.O. 2012. Characterization of iNOS(+) Neutrophil-like ring cell in tumor-bearing mice. *J Transl Med* 10:152.

30. Hart, K.M., Usherwood, E.J., and Berwin, B.L. 2014. CX3CR1 delineates temporally and functionally distinct subsets of myeloid-derived suppressor cells in a mouse model of ovarian cancer. *Immunol Cell Biol* 92: 499-508.

31. Mazzoni, A., Bronte, V., Visintin, A., Spitzer, J.H., Apolloni, E., Serafini, P., Zanovello, P., and Segal, D.M. 2002. Myeloid suppressor lines inhibit T cell responses by an NO-dependent mechanism. *J Immunol* 168: 689-695.

32. Dolcetti, L., Peranzoni, E., Ugel, S., Marigo, I., Fernandez Gomez, A., Mesa, C., Geilich, M., Winkels, G., Traggiai, E., Casati, A., et al. 2010. Hierarchy of

636 immunosuppressive strength among myeloid-derived suppressor cell subsets is
637 determined by GM-CSF. *European Journal of Immunology* 40: 22-35.
638 33. Sawanobori, Y., Ueha, S., Kurachi, M., Shimaoka, T., Talmadge, J.E., Abe, J.,
639 Shono, Y., Kitabatake, M., Kakimi, K., Mukaida, N., et al. 2008.
640 Chemokine-mediated rapid turnover of myeloid-derived suppressor cells in
641 tumor-bearing mice. *Blood* 111: 5457-5466.
642 34. Song, X., Krelin, Y., Dvorkin, T., Bjorkdahl, O., Segal, S., Dinarello, C.A., Voronov,
643 E., and Apte, R.N. 2005. CD11b+/Gr-1+ Immature Myeloid Cells Mediate
644 Suppression of T Cells in Mice Bearing Tumors of IL-1β-Secreting Cells. *The*
645 *Journal of Immunology* 175: 8200-8208.
646 35. Schreck, R., and Baeuerle, P.A. 1990. NF-kappa B as inducible transcriptional
647 activator of the granulocyte-macrophage colony-stimulating factor gene. *Molecular*
648 *and Cellular Biology* 10: 1281-1286.
649 36. Thomas, R.S., Tymms, M.J., McKinlay, L.H., Shannon, M.F., Seth, A., and Kola, I.
650 1997. ETS1, NFkappaB and AP1 synergistically transactivate the human GM-CSF
651 promoter. *Oncogene* 14: 2845-2855.
652 37. Suzuki, E., Kapoor, V., Jassar, A.S., Kaiser, L.R., and Albelda, S.M. 2005.
653 Gemcitabine Selectively Eliminates Splenic Gr-1+/CD11b+ Myeloid Suppressor

654 Cells in Tumor-Bearing Animals and Enhances Antitumor Immune Activity. *Clinical*
655 *Cancer Research* 11: 6713-6721.
656 38. Dumitru, C.A., Moses, K., Trellakis, S., Lang, S., and Brandau, S. 2012.
657 Neutrophils and granulocytic myeloid-derived suppressor cells:
658 immunophenotyping, cell biology and clinical relevance in human oncology.
659 *Cancer Immunol Immunother* 61: 1155-1167.
660 39. Ryan, D.P., Hong, T.S., and Bardeesy, N. 2014. Pancreatic Adenocarcinoma.
661 *New England Journal of Medicine* 371: 1039-1049.
662 40. White, R.R., and Evans, D.B. 2014. Neoadjuvant chemotherapy for localized
663 pancreatic cancer: too little or too long? *Ann Surg Oncol* 21: 1508-1509.
664 41. Boeck, S., Haas, M., Ormanns, S., Kruger, S., Siveke, J.T., and Heinemann, V.
665 2014. Neoadjuvant chemotherapy in pancreatic cancer: innovative, but still difficult.
666 *Br J Cancer*.
667 42. Tsuchikawa, T., Md, M.M., Yamamura, Y., Shichinohe, T., Hirano, S., and Kondo,
668 S. 2011. The Immunological Impact of Neoadjuvant Chemotherapy on the Tumor
669 Microenvironment of Esophageal Squamous Cell Carcinoma. *Ann Surg Oncol*.
670 43. Homma, Y., Taniguchi, K., Murakami, T., Nakagawa, K., Nakazawa, M.,
671 Matsuyama, R., Mori, R., Takeda, K., Ueda, M., Ichikawa, Y., et al. 2014.
672 Immunological impact of neoadjuvant chemoradiotherapy in patients with

673 borderline resectable pancreatic ductal adenocarcinoma. *Ann Surg Oncol* 21:
674 670-676.
675 44. Halama, N., Michel, S., Kloor, M., Zoernig, I., Benner, A., Spille, A., Pommerencke,
676 T., von Knebel, D.M., Folprecht, G., Luber, B., et al. 2011. Localization and
677 Density of Immune Cells in the Invasive Margin of Human Colorectal Cancer Liver
678 Metastases Are Prognostic for Response to Chemotherapy. *Cancer Research* 71:
679 5670-5677.
680 45. Qian, B.-Z., and Pollard, J.W. 2010. Macrophage Diversity Enhances Tumor
681 Progression and Metastasis. *Cell* 141: 39-51.
682 46. Lyden, D., Hattori, K., Dias, S., Costa, C., Blaikie, P., Butros, L., Chadburn, A.,
683 Heissig, B., Marks, W., Witte, L., et al. 2001. Impaired recruitment of
684 bone-marrow-derived endothelial and hematopoietic precursor cells blocks tumor
685 angiogenesis and growth. *Nat Med* 7: 1194-1201.
686 47. Gilbert, L.A., and Hemann, M.T. 2010. DNA Damage-Mediated Induction of a
687 Chemoresistant Niche. *Cell* 143: 355-366.
688 48. Middleton, G., Silcocks, P., Cox, T., Valle, J., Wadsley, J., Propper, D., Coxon, F.,
689 Ross, P., Madhusudan, S., Roques, T., et al. 2014. Gemcitabine and capecitabine
690 with or without telomerase peptide vaccine GV1001 in patients with locally

691 advanced or metastatic pancreatic cancer (TeloVac): an open-label, randomised,
692 phase 3 trial. *Lancet Oncol* 15: 829-840.
693 49. Vernon, P.J., Loux, T.J., Schapiro, N.E., Kang, R., Muthuswamy, R., Kalinski, P.,
694 Tang, D., Lotze, M.T., and Zeh, H.J. 2013. The Receptor for Advanced Glycation
695 End Products Promotes Pancreatic Carcinogenesis and Accumulation of
696 Myeloid-Derived Suppressor Cells. *The Journal of Immunology* 190: 1372-1379.
697 50. Krysko, O., Love Aaes, T., Bachert, C., Vandenabeele, P., and Krysko, D.V. 2013.
698 Many faces of DAMPs in cancer therapy. *Cell Death Dis* 4:e631.

Figure Legend

Figure.1 Supernatants of human PDAC cell culture induce the differentiation of monocytes into MDSCs

(A) A scheme of culture protocol used to study the effects of PDAC-derived factors on monocytes differentiation. Human peripheral $CD14^+$ monocytes were purified from healthy donor and cultured in PDAC CM for 6 days. (B) Representative photomicrographs of monocytes cultured for 6 days in normal medium, Capan-1 CM or PANC-1 CM. Monocytes differentiate into spindle macrophage-like cells when cultured in normal medium, whereas the supernatants of PDAC cells induce monocytes differentiation into circular immature cells. Scale bars: 100μm. (C) Flow cytometry analysis of CD14, CD33 and HLA-DR expression in monocytes cultured in normal medium (control), Capan-1 CM or PANC-1 CM. PDAC CM-treated monocytes were $CD14^+CD33^+HLA\text{-}DR^{low}$ cells resembling mo-MDSC. (D) HLA-DR expression levels in cultured monocytes at day 6. HLA-DR expressions was significantly decreased when monocytes were cultured in PDAC CM (*n*=3 donors). (E) Flow cytometry analysis of NOS2 and ARG1 in monocytes cultured in normal medium (control), Capan-1 or PANC-1 CM. Gray histogram: isotype, black line: control medium, gray line: Capan-1 or PANC-1 CM. Capan-1 or PANC-1 CM-treated monocytes show high levels of NOS2 and ARG1 compared to control. (F) Flow

718 cytometry analysis of CD11b, CD15, CCR2 and CXCR1 expression in monocytes
719 cultured in Capan-1 or PANC-1 CM. Gray histogram: isotype, black line: Capan-1 or
720 PANC-1 CM. PDAC CM-treated monocytes showed expression of CD11b and CCR2
721 but lack the expression of CD15 or CXCR1. Flowcytometry results are shown as
722 representative multiple independent experiments. $^{*}P < 0.05$; $^{**}P < 0.01$.
723
724 **Figure.2 Supernatants of chemotherapy-treated PDAC cells induce**
725 **morphological changes in monocytes with enhanced MDSC markers**
726 (A) A scheme of culture protocol used to study the effects of chemotherapy-treated
727 PDAC microenvironment on monocytes differentiation. Capan-1 cells were pulsed
728 with GEM (1μM or 30μM) or 5-FU (10μg/ml) for 1 hour, followed by careful wash with
729 sterilized PBS, and change into fresh medium. Conditioned medium was collected
730 after 72 hour and applied to human peripheral $CD14^{+}$ monocytes as described above.
731 (B) Morphological changes in monocytes cultured in GEM-treated PDAC CM at day 6.
732 These cells were larger in size than monocytes cultured in PBS-treated PDAC CM.
733 Scale pars: 100μm. (C) May Giemsa staining showed unique cytoplasmic vacuoles in
734 monocytes cultured in GEM-treated PDAC CM (red arrows) but not PBS-treated
735 PDAC CM or normal medium. Scale bars: 20μm (D and E) Flowcytometry analysis
736 shows high forward and side scatter voltage signals (upper panel) and increased

frequencies of HLA-DR$^{low/negative}$ fraction (lower panel) in monocytes cultured in GEM-treated PDAC CM compared to PBS-treated PDAC CM. (*n*=3 donors). (F) Enhanced expression of NOS2 in monocytes cultured in the supernatants of GEM-treated Capan-1 cells. Data are shown as representative of 2 independent experiments. $^{*}P < 0.05$; $^{**}P < 0.01$.

Figure.3 Chemotherapy treatment amplifies the expression of multiple MDSCs-inducing cytokines in PDAC cells via MAPK pathway-mediated signal

(A) and (B) Quantitative RT-PCR analysis for various cytokines and chemokines in PBS or GEM-treated (A) or 5-FU-treated (B) Capan-1 cells after 72 hours of stimulation. Data from PBS-treated cells were set as 1. Data is shown as representative of 3 independent experiments. (C) ELISA measurement of GM-CSF in the supernatants of PBS or chemotherapy-treaded Capan-1 cells after 72 hours of stimulation. GM-CSF production is enhanced after chemotherapy treatment in a dose-dependent manner. Data is shown as representative of 2 independent experiments. (D) Western blotting of p-ERK or total ERK, p-AKT or total AKT, and β-Actin of PBS or GEM-treated Capan-1 cells stimulated for the indicated time. GEM enhances the phosphorylation of ERK in a time-dependent manner. Similar results were obtained from multiple independent experiments. (E) A time course of luciferase

activity of *Nfκb* promoter-luciferase reporter plasmid in Capan-1 cells stimulated with GEM (upper panel) or f-FU (lower panel). Data is shown as representative of 2 independent experiments. $^{*}P < 0.05$; $^{**}P < 0.01$; $^{***}P < 0.001$.

Figure.4 Blockade of GM-CSF contributes to the reversal of morphological and phenotypic changes induced in monocytes by chemotherapy-treated PDAC CM

(A) Flowcytometry analysis shows decreased forward and side scatter voltage signals (upper panel) and decreased frequencies of HLA-$DR^{low/negative}$ fraction (lower panel) in monocytes cultured in GEM-treated PDAC CM after depletion of GM-CSF (anti-GM-CSF: 10μg/ml). (B) Microscopic examination and May Giemsa staining showed decrease in cell size (upper panel) and disappearance of cytoplasmic vacuoles (lower panel) that were observed in GEM-treated PDAC CM after treatment with anti-GM-CSF. Scale bars: 100μm for photomicrographs and 20μm for May Giemsa staining. (C) Photomicrographs of T cell aggregate. MDSCs were co-cultured with autologous $CD4^{+}$ T cells stimulated with anti-CD3/28 for 72 hours at the indicated ratio. Data are shown as representative of two independent experiments. Scale bar: 10μm. (D) T cell proliferation assay. MDSCs were co-cultured with autologous $CD4^{+}$ T cells stimulated with anti-CD3/28 for 72 hours at the indicated ratio, and T cell proliferation was measured by H^{3} thymidine uptake. Neutralization of GM-CSF in

775 GEM-treated Capan-1 CM was effective to abolish the immunosuppressive functions
776 and contribute to the recovery of $CD4^+$ T cell function as observed by enhanced
777 aggregation and proliferation. Data are shown as representative of two independent
778 experiments. $^{*}P < 0.05$; $^{**}P < 0.01$; $^{***}P < 0.001$.
779
780 **Figure.5 GM-CSF expression is observed in various PDAC cell lines and tumor**
781 **tissues of PDAC patients, and related to the enhancement of MDSC markers**
782 **after treatment with pre-operative chemotherapy**
783 (A) Quantitative RT-PCR analysis of GM-CSF in various PDAC cell and non-PDAC
784 cell lines. GM-CSF expression was normalized to GAPDH. Data is shown as
785 representative of 3 independent experiments. (B) Immunohistochemistry staining of
786 GM-CSF in PDAC region or normal region of pancreatic tissues from PDAC patients.
787 Scale bar: 100μm. (C) The intensity of GM-CSF staining was classified according to a
788 three-level scale: 0, 1+, 2+ and 71% of patients were GM-CSF high criteria. (D)
789 Kaplan-Meier survival analysis of overall survival in 68 resected PDAC samples.
790 GM-CSF-high population showed significantly lower survival rates. (E)
791 Immunohistochemistry staining of CD14 and HLA-DR in pancreatic tissues of PDAC
792 patients before or after treatment with pre-operative chemotherapy. Scale bar: 100μm.
793 (F) Frequencies of $CD14^+HLA\text{-}DR^+$ (left) and percentage of $HLA\text{-}DR^+$ cells to total

794 $CD14^+$ cells (middle) and total $CD14^+$ (right) in pancreatic tissues of PDAC patients
795 before or after pre-operative chemotherapy. (G) Immunohistochemistry staining of
796 CD66b in pancreatic tissues of PDAC patients before or after treatment with
797 pre-operative chemotherapy. Scale bar: 100μm. (H) Frequencies of $CD66b^+$ in
798 pancreatic tissues of PDAC patients before or after pre-operative chemotherapy. For
799 F and H, bars indicate the median value and the box encompasses the 25^{th} and 75^{th}
800 percentiles. * $P < 0.05$; ** $P < 0.01$; *** $P < 0.001$.
801
802 **Figure.6 Mechanism of chemotherapy-mediated induction of MDSCs**
803 A scheme of mechanism by which chemotherapy induces MDSC formation in PDAC
804 microenvironment is shown. Chemotherapy induces activation of MAPK signal
805 pathway and NF-κB promoter activities leading to enhancement in GM-CSF
806 production which in turn enhance the differentiation of monocytes into MDSCs.
807 Anti-GM-CSF Ab may offer a promising tool to block monocytes differentiation into
808 MDSCs, and thus help the recovery of effective antitumor T cell response.

Supplementary Figure Legend

Supplementary figure.1 5-FU-treated Capan-1 supernatants induce the differentiation of monocytes into MDSCs

Flow cytometry analysis of FSC, SSC and HLA-DR expression in monocytes cultured in normal medium (control), 5-FU- treated Capan-1 CM.

Supplementary figure.2 Gemcitabine amplifies the expression of multiple MDSCs-inducing cytokines including GM-CSF in PANC-1 cell line

Quantitative RT-PCR analysis of various cytokines and chemokines in PBS- or GEM-treated PANC-1 cells after 72 hours of stimulation. Data from PBS-treated cells were set as 1. Data is shown as representative of 3 independent experiments. $^{*}P < 0.05$; $^{**}P < 0.01$; $^{***}P < 0.001$.

Supplementary figure.3 Gemcitabine amplifies the expression of IL-6 or IL8 in Capan-1 cells

ELISA measurement of IL-6 and IL-8 in the supernatants of PBS- or GEM-treaded Capan-1 cells after 72 hours of stimulation. Both cytokine productions were enhanced after GEM treatment in a dose-dependent manner. Data is shown as representative of 2 independent experiments.

828

829 **Supplementary figure.4 Blockade of GM-CSF contributes to the recovery of**
830 **$CD8^+$ T cells proliferation when cultured with monocytes stimulated with**
831 **chemotherapy-treated PDAC CM**

832 (A) Photomicrographs of T cell aggregate. $CD8^+$ T cells stimulated with anti-CD3/28
833 were co-cultured with autologous MDSCs for 72 hours at the indicated ratio.
834 Representative of two independent experiments. Scale bar: 10μm. (B) $CD8^+$ T cell
835 proliferation was measured by H^3 thymidine uptake. Neutralization of GM-CSF in
836 GEM-treated Capan-1 CM contribute to the recovery of $CD8^+$ T cell proliferation. Data
837 are shown as representative of two independent experiments. $^{*}P < 0.05$; $^{**}P < 0.01$;
838 $^{***}P < 0.001$.

839

840 **Supplementary figure.5 No significant difference in the frequencies of $CD68^+$**
841 **macrophages in cancer patients after treatment with pre-operative**
842 **chemotherapy**

843 Frequencies of $CD68^+$ cells in pancreatic tissues of PDAC patients before or after
844 pre-operative chemotherapy.

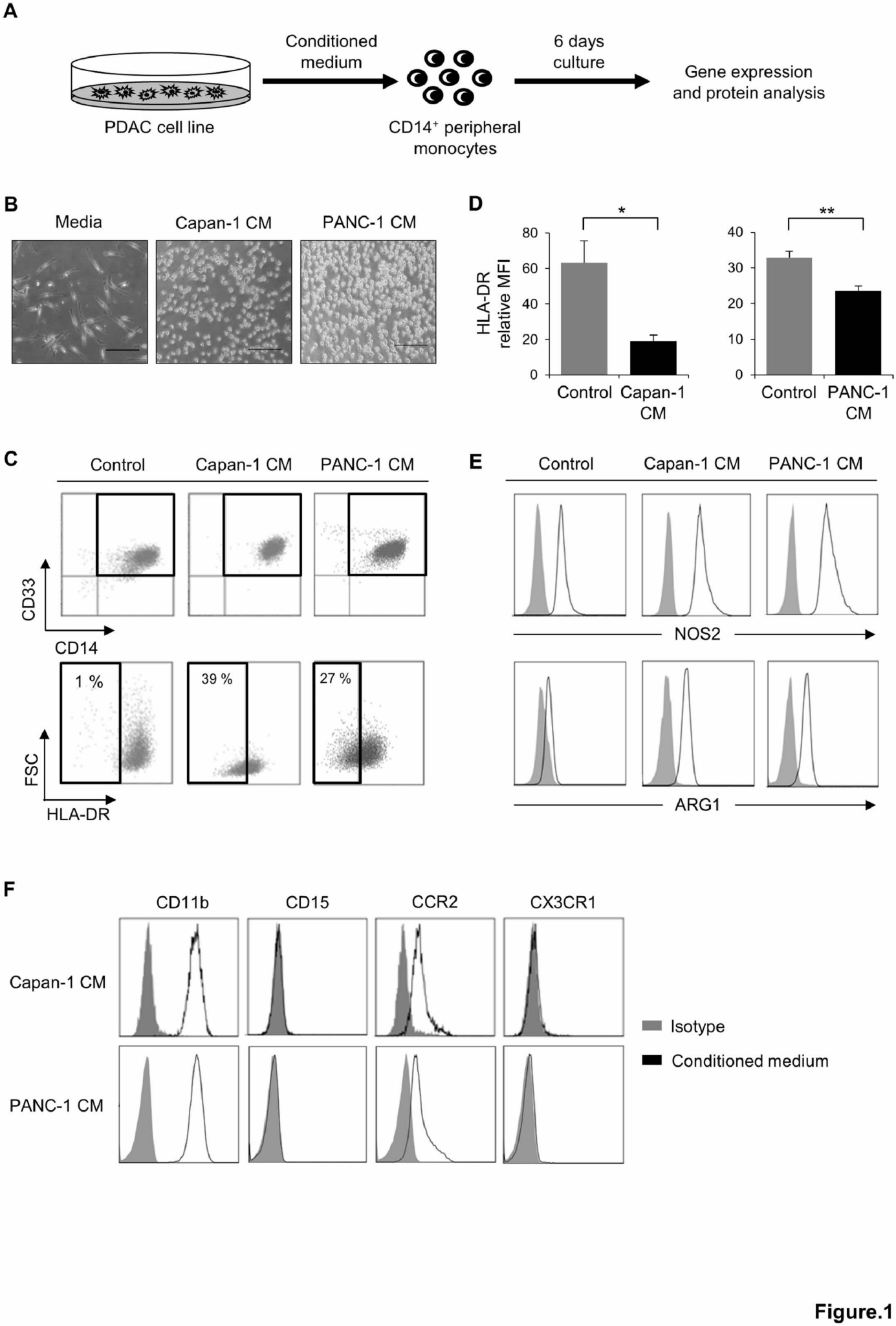
A
Conditioned medium
6 days culture
Gene expression and protein analysis
PDAC cell line
CD14+ peripheral monocytes
B
Media
Capan-1 CM
PANC-1 CM
D
HLA-DR relative MFI
*
**
Control
Capan-1 CM
PANC-1 CM
C
Control
Capan-1 CM
PANC-1 CM
CD33
CD14
1 %
39 %
27 %
FSC
HLA-DR
E
Control
Capan-1 CM
PANC-1 CM
NOS2
ARG1
F
CD11b
CD15
CCR2
CX3CR1
Capan-1 CM
PANC-1 CM
Isotype
Conditioned medium

Figure.1

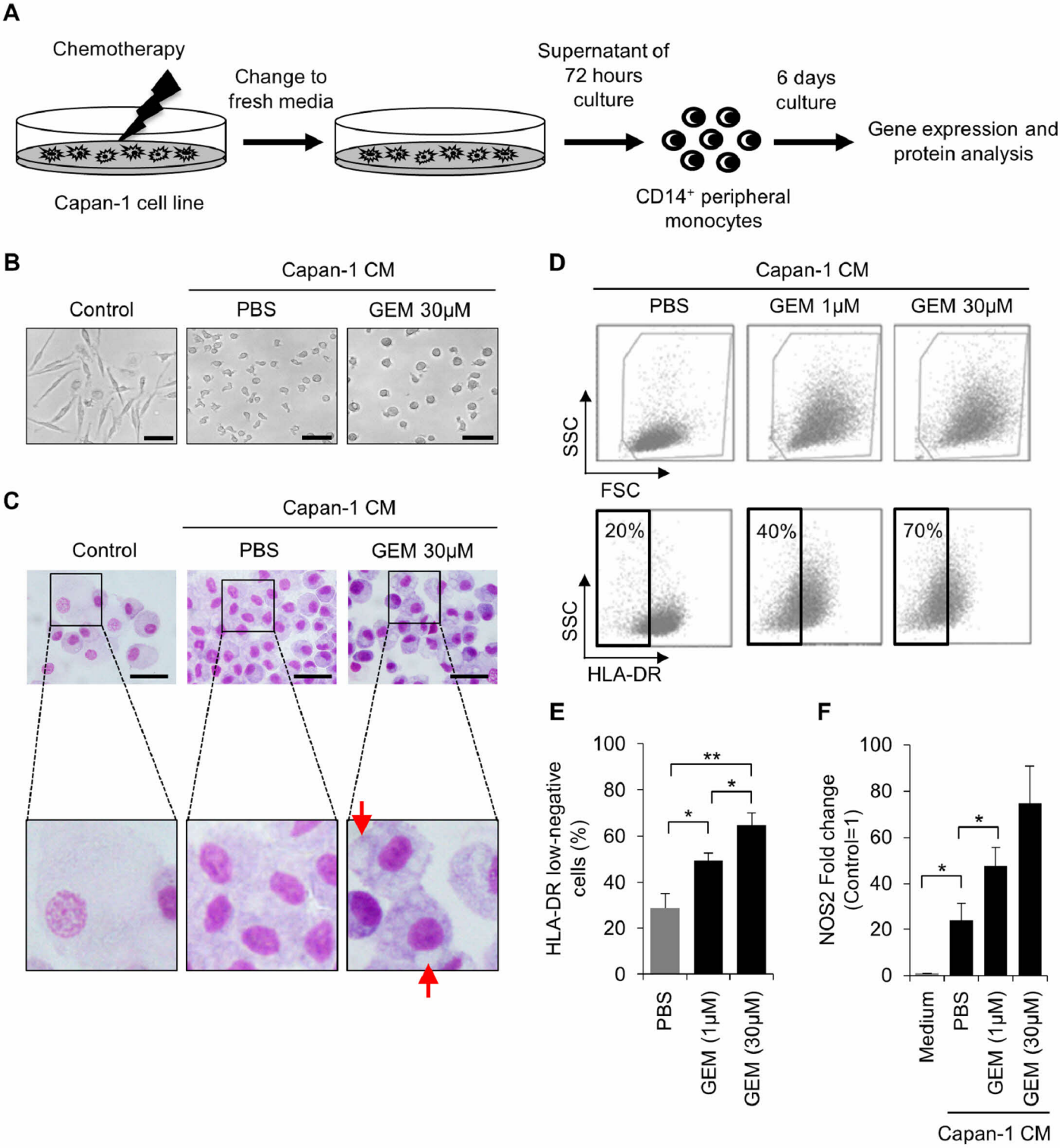
A
Chemotherapy
Change to fresh media
Supernatant of 72 hours culture
6 days culture
Gene expression and protein analysis
Capan-1 cell line
CD14+ peripheral monocytes
B
Capan-1 CM
Control
PBS
GEM 30μM
C
Capan-1 CM
Control
PBS
GEM 30μM
D
Capan-1 CM
PBS
GEM 1μM
GEM 30μM
SSC
FSC
20%
40%
70%
SSC
HLA-DR
E
HLA-DR low-negative cells (%)
100
80
60
40
20
0
**
*
*
PBS
GEM (1μM)
GEM (30μM)
F
NOS2 Fold change (Control=1)
100
80
60
40
20
0
*
*
Medium
PBS
GEM (1μM)
GEM (30μM)
Capan-1 CM

Figure.2

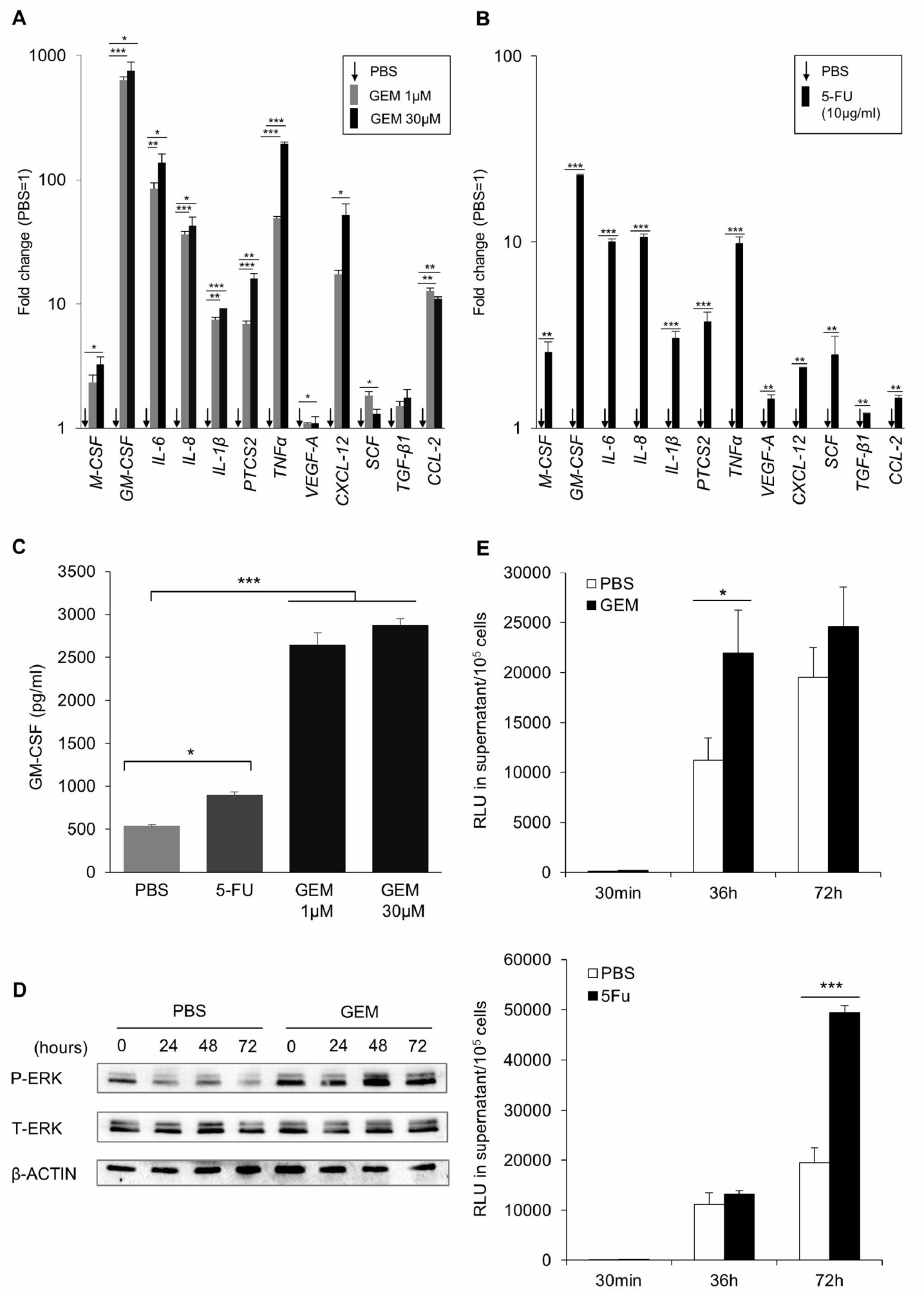
A
Fold change (PBS=1)
PBS
GEM 1μM
GEM 30μM
M-CSF
GM-CSF
IL-6
IL-8
IL-1β
PTCS2
TNFα
VEGF-A
CXCL-12
SCF
TGF-β1
CCL-2
B
Fold change (PBS=1)
PBS
5-FU (10μg/ml)
C
GM-CSF (pg/ml)
PBS
5-FU
GEM 1μM
GEM 30μM
D
PBS
GEM
(hours)
0
24
48
72
P-ERK
T-ERK
β-ACTIN
E
RLU in supernatant/10^5 cells
PBS
GEM
30min
36h
72h
RLU in supernatant/10^5 cells
PBS
5Fu
30min
36h
72h

Figure.3

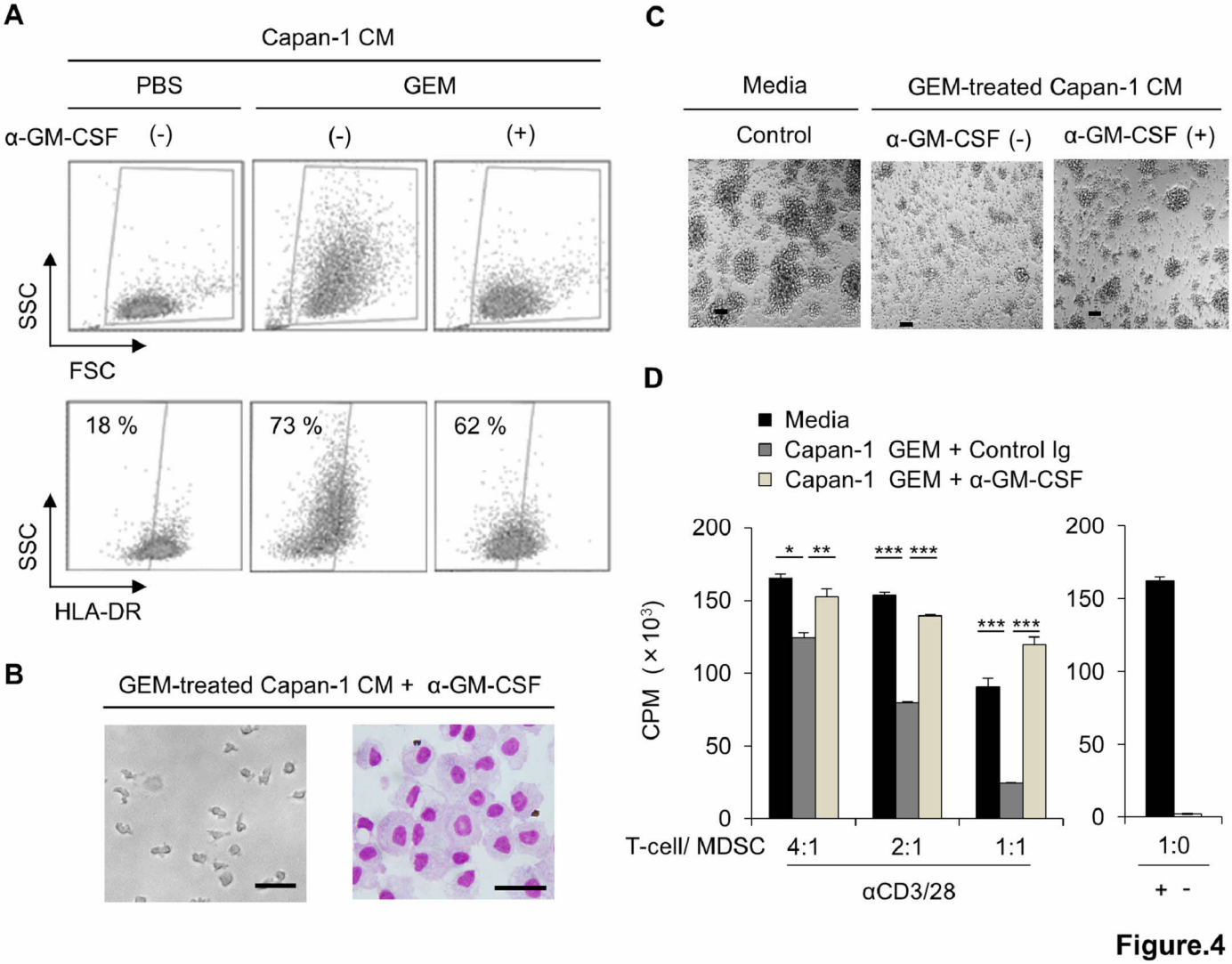
A
Capan-1 CM
PBS
GEM
α-GM-CSF (-) (-) (+)
SSC
FSC
18 %
73 %
62 %
SSC
HLA-DR
B
GEM-treated Capan-1 CM + α-GM-CSF
C
Media
GEM-treated Capan-1 CM
Control
α-GM-CSF (-)
α-GM-CSF (+)
D
Media
Capan-1 GEM + Control Ig
Capan-1 GEM + α-GM-CSF
CPM (×10³)
200
150
100
50
0
* **
*** ***
*** ***
T-cell/ MDSC 4:1 2:1 1:1 1:0
αCD3/28
+ -

Figure.4

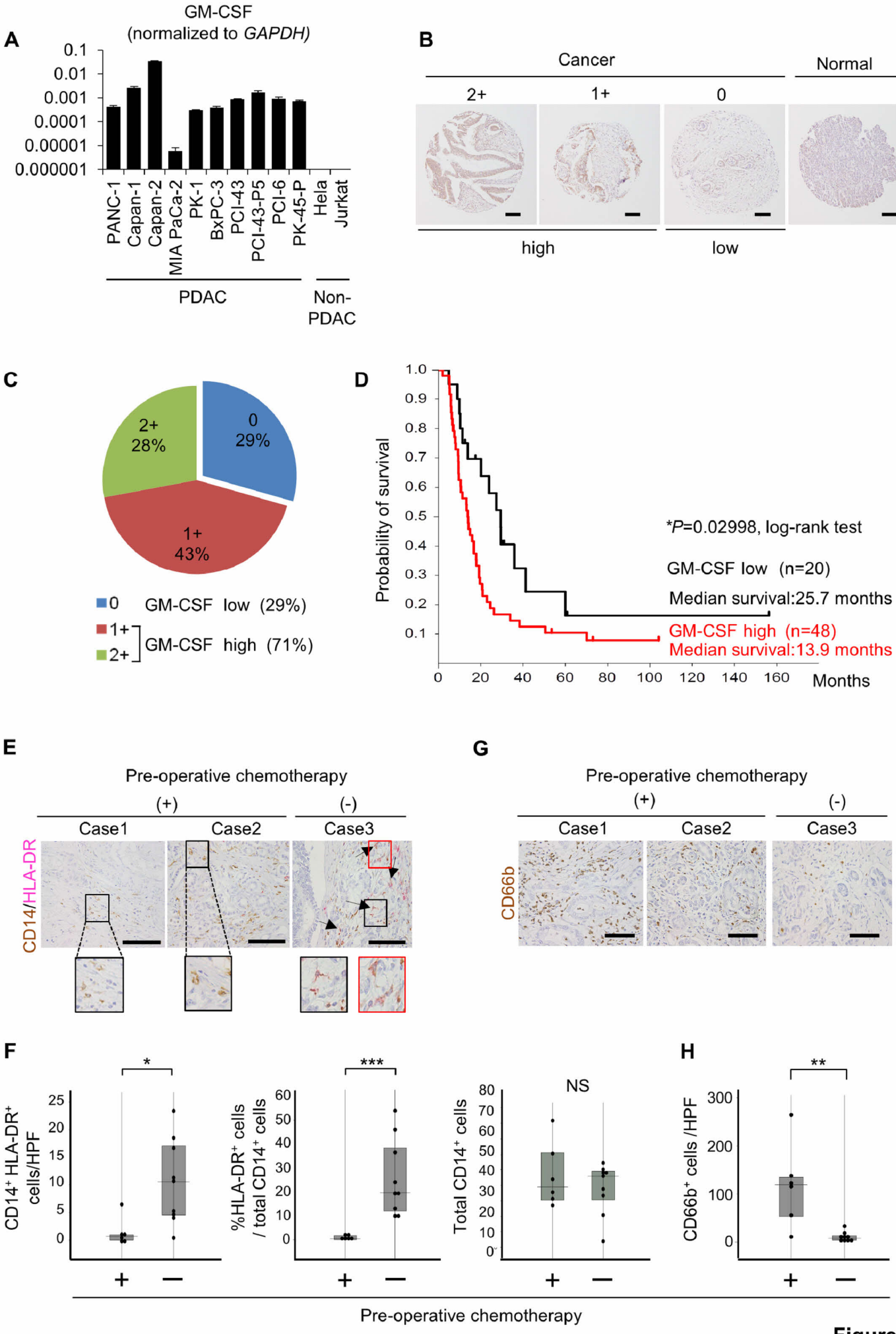
A
GM-CSF
(normalized to GAPDH)
0.1
0.01
0.001
0.0001
0.00001
0.000001
PANC-1
Capan-1
Capan-2
MIA PaCa-2
PK-1
BxPC-3
PCI-43
PCI-43-P5
PCI-6
PK-45-P
Hela
Jurkat
PDAC
Non-PDAC
B
Cancer
Normal
2+
1+
0
high
low
C
2+ 28%
0 29%
1+ 43%
0 GM-CSF low (29%)
1+
2+
GM-CSF high (71%)
D
Probability of survival
1.0
0.9
0.8
0.7
0.6
0.5
0.4
0.3
0.2
0.1
0
20
40
60
80
100
120
140
160
Months
*P=0.02998, log-rank test
GM-CSF low (n=20)
Median survival:25.7 months
GM-CSF high (n=48)
Median survival:13.9 months
E
Pre-operative chemotherapy
(+)
(-)
Case1
Case2
Case3
CD14/HLA-DR
G
Pre-operative chemotherapy
(+)
(-)
Case1
Case2
Case3
CD66b
F
CD14+ HLA-DR+ cells/HPF
*
%HLA-DR+ cells / total CD14+ cells
***
Total CD14+ cells
NS
H
CD66b+ cells /HPF
**
+
−
Pre-operative chemotherapy

Figure.5

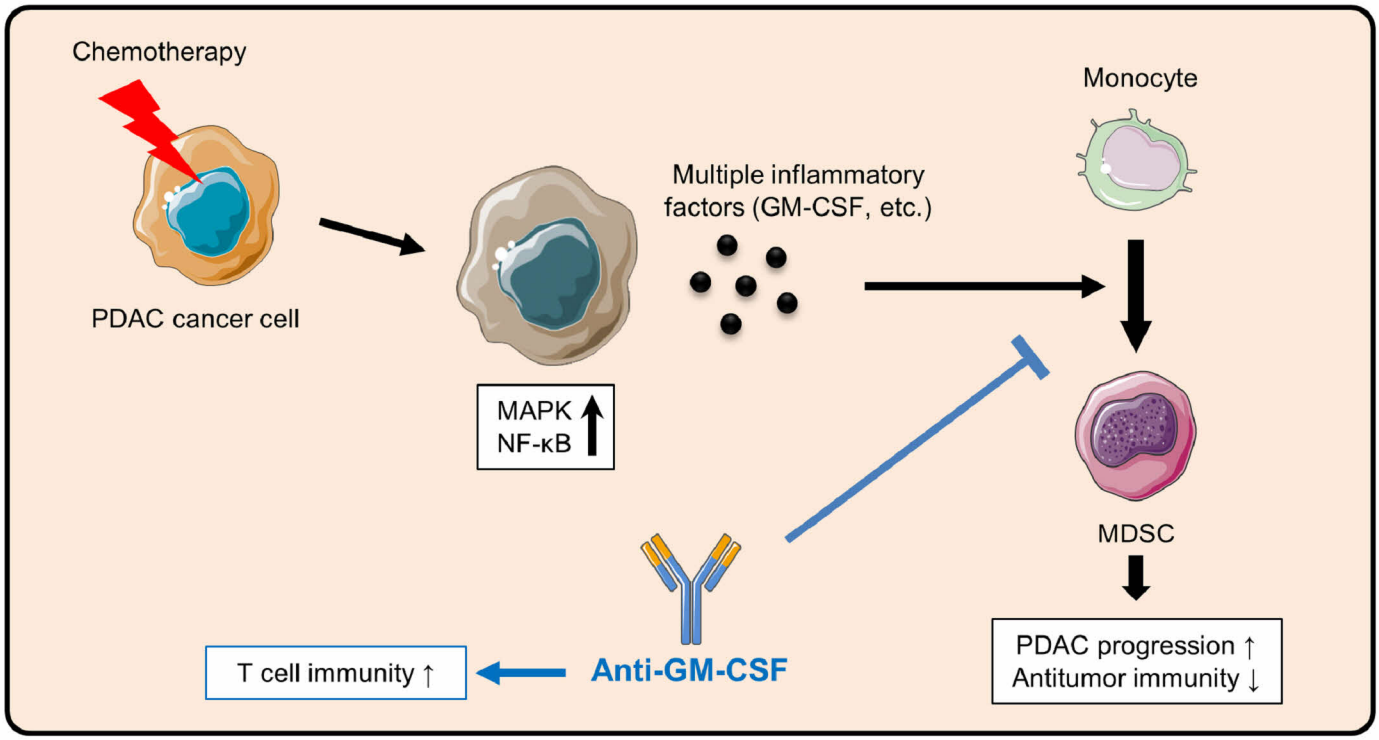
Chemotherapy
PDAC cancer cell
MAPK
NF-κB
Multiple inflammatory
factors (GM-CSF, etc.)
Monocyte
MDSC
PDAC progression ↑
Antitumor immunity ↓
Anti-GM-CSF
T cell immunity ↑

Figure.6